AD-A081 989 AERODYNE RESEARCH INC BEDFORD MA F/G 4/1
ANALYSIS AND MODELLING OF THE DIRT I AND GRAF II BATTLEFIELD DU--ETC(U)
JAN 80 J F EBERSOLE, R VAGLIO-LAURIN TCN-79-105
UNCLASSIFIED ARI-RR-168 ERADCOM/ASL-CR-80-1137-1 NL

END
DATE FILMED
4-80
DTIC

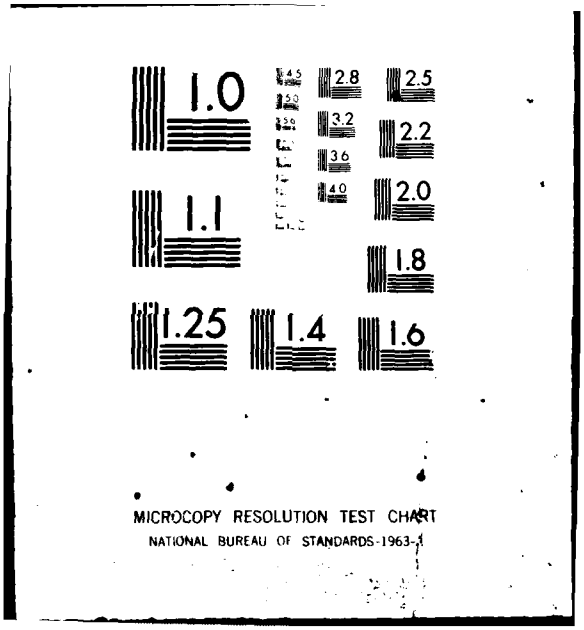
1.0
1.1
1.25
1.4
1.6
1.8
2.0
2.2
2.5
2.8
3.2
3.6
4.0
MICROCOPY RESOLUTION TEST CHART
NATIONAL BUREAU OF STANDARDS-1963-A

ASL-CR-80-1137-1

AD

Reports Control Symbol
OSD 1366

LEVEL II

ANALYSIS AND MODELLING OF THE DIRT I AND GRAF II BATTLEFIELD DUST OBSCURATION DATA

JANUARY 1980

Prepared by

JOHN F. EBERSOLE
ROBERTO VAGLIO-LAURIN
DAVID S. DVORE
MANUEL MARTINEZ-SANCHEZ

Aerodyne Research, Inc.
Bedford Research Park
Crosby Drive
Bedford, MA 01730

Under Contract TCN-79-105/D.O.-1137
CONTRACT MONITOR: LOUIS DUNCAN

Approved for public release; distribution unlimited

US Army Electronics Research and Development Command
ATMOSPHERIC SCIENCES LABORATORY
White Sands Missile Range, NM 88002

NOTICES

Disclaimers

The findings in this report are not to be construed as an official Department of the Army position, unless so designated by other authorized documents.

The citation of trade names and names of manufacturers in this report is not to be construed as official Government indorsement or approval of commercial products or services referenced herein.

Disposition

Destory this report when it is no longer needed. Do not return it to the originator.

UNCLASSIFIED

SECURITY CLASSIFICATION OF THIS PAGE (When Data Entered)

REPORT DOCUMENTATION PAGE

READ INSTRUCTIONS BEFORE COMPLETING FORM

1. REPORT NUMBER: ASL-CR-80-1137-1	2. GOVT ACCESSION NO.
3. RECIPIENT'S CATALOG NUMBER	
4. TITLE (and Subtitle): ANALYSIS AND MODELLING OF THE DIRT I AND GRAF II BATTLEFIELD DUST OBSCURATION DATA	5. TYPE OF REPORT & PERIOD COVERED: Final Report • Jan [illegible] - Jun[illegible] 1979
6. PERFORMING ORG. REPORT NUMBER: ARI-RR-168	
7. AUTHOR(s): John F. Ebersole, Roberto Vaglio-Laurin, David S. Dvore, Manuel Martinez-Sanchez	8. CONTRACT OR GRANT NUMBER(s): TCN-79-105/D.O. 1137
9. PERFORMING ORGANIZATION NAME AND ADDRESS: Aerodyne Research, Inc., Bedford Research Park, Crosby Drive, Bedford, MA 01730	10. PROGRAM ELEMENT, PROJECT, TASK AREA & WORK UNIT NUMBERS: 61102A-1L161102B53A[illegible] 13
11. CONTROLLING OFFICE NAME AND ADDRESS: Dr. Louis Duncan, Atmospheric Sciences Laboratory, White Sands Missile Range, N. M.	12. REPORT DATE: Jan[illegible] 1980
	13. NUMBER OF PAGES: 41
14. MONITORING AGENCY NAME & ADDRESS (if different from Controlling Office)	15. SECURITY CLASS. (of this report): Unclassified
	15a. DECLASSIFICATION/DOWNGRADING SCHEDULE

16. DISTRIBUTION STATEMENT (of this Report)

Approved for public release; distribution unlimited

17. DISTRIBUTION STATEMENT (of the abstract entered in Block 20, if different from Report)

18. SUPPLEMENTARY NOTES

Contract Monitor: Louis Duncan

19. KEY WORDS (Continue on reverse side if necessary and identify by block number)

Dust, aerosol, obscuration, transmission, atmospheric diffusion, wind shear, gravitational settling, explosions, battlefield clutter, DIRT I test, Graf II test

20. ABSTRACT (Continue on reverse side if necessary and identify by block number)

An analysis of photographic information is used to determine the source characteristics and the salient aspects of atmospheric diffusion for explosion-produced dust clouds. Specifically, the dependence of source strength (dust yield) upon the nature of the terrain and surface vegetative cover (sod) is identified. A partitioning of ejecta into essentially two distinct clouds, only one of which is buoyantly rising, is noted. Analytic solutions describing the diffusion of these two clouds taking into account the effects of vertical wind shear and gravitational settling are presented. →

DD FORM 1 JAN 73 1473 EDITION OF 1 NOV 65 IS OBSOLETE
S/N 0102-LF-014-6601

UNCLASSIFIED
SECURITY CLASSIFICATION OF THIS PAGE (When Data Entered)

Abstract (Cont.)

Finally, experimental evidence indicative of large obscuration amplitude modulations is discussed and its association with effects due to large atmospheric eddies is suggested. This work on aerosol source characterization and the atmospheric diffusion solutions is part of the validation of the Aerodyne Research, Inc. Disturbed Infrared Transmission Model DIRTRAN which will be incorporated into the Electro-Optical Systems Atmospheric Effects Library (EO-SAEL) at the Army Atmospheric Sciences Laboratory, White Sands Missile Range, N.M.

TABLE OF CONTENTS

Section		Page
1	INTRODUCTION	1
2	AEROSOL SOURCE TERM: EXPLOSION-PRODUCED DUST	4
	2A. Crater Ejecta	4
	2B. Effect of Vegetative Cover on Production of Dust Clouds	4
	2C. Partitioning of Particles Inside and Outside of the Explosion Fireball	12
	2D. Initial Hot Gas Cloud	12
3	ATMOSPHERIC DIFFUSION	16
	3A. Buoyant Cloud Rise and Diffusion	16
	3B. Wind-Controlled Diffusion	16
4	IR CLUTTER	26
5	SUMMARY AND CONCLUSIONS	33
	Acknowledgements	34
	References	35

LIST OF ILLUSTRATIONS

Figure		Page
1	Example of a Clutter in a Battlefield Scenario	2
2	Elements of the Aerodyne DIRTRAN (Disturbed Infrared Transmission) Model	3
3	Nomograph for Determining the Apparent Crater Radius R in Various Media	5
4	Nomograph Similar to Figure 3 But Used for Determining the Apparent Crater Depth d in Various Media	6
5	Transmission in the 8 - 12 μm Band During a 155 mm HE Barrage at Ft. Knox, Ky.	7
6	Transmission in the 8 - 12 μm and 0.8 - 1.1 μm Band During a 155 mm HE Barrage at Grafenwohr, Germany	8
7	Graf II Test 155 mm HE Round Craters	10
8	Effect of Sod (Vegetative Cover) on Crater Volume	11
9	Example of Entrainment Partitioning of Explosion-Produced Soil Ejecta Inside and Outside of Hot Gases From Explosion	14
10	Example of Buoyant Rise Effects on the Dispersion of Explosion-Produced Dust Clouds	15
11	Example of wind-controlled diffusion of dust clouds produced by artillery explosions occurring in the Dust/Debris Test conducted by Dugway Proving Ground at Ft. Sill, Ok, May 1978	17
12	Wind controlled aerosol dispersion	24
13	Buoyancy diffusion of aerosols with wind and gravitational settling (50 μm diameter particles)	24
14	Superposition of wind and buoyancy controlled diffusion of small particles	25

List of Illustrations (Cont.)

Figure		Page
15	Effect of large-eddy turbulence on visibility holes	27
16	Example of visibility holes produced by the interplay of large-eddy turbulence effects and fire smoke generation on obscuration	29
17	Two pictures of buoyantly rising smoke separated in time by approximately 40 sec	30
18	Example of bifurcation of DIRT I fire smoke clouds due to large atmospheric eddies separated in time by approximately 20 sec.	31
19	View of approximately the same "wishbone" fire smoke event (temporal separation of less than 2.5 sec) from two different aspects (angular separation of 64.2^{o})	32

1. INTRODUCTION

As indicated in Figure 1, the problem we are addressing is that of battlefield clutter due to the presence of aerosols and atmospheric motion produced by turbulence and rapidly moving hot air. We have a variety of aerosol sources such as dirt kicked up by explosions, dust clouds due to wind storms and vehicular motion, haze and fog, smoke from fires, and screening smokes. Each of these aerosol sources contributes serious degradation to the operation of electro-optical systems. Our work has been directed towards describing and developing an understanding of the various aerosol source terms and their subsequent diffusion in the atmosphere. From this, we have been developing a disturbed IR transmission (DIRTRAN) model to describe the degradation effects produced by battlefield clutter.[1-6] Validation of this model is being performed with the aid of data obtained at several recent Army infrared obscuration field trials.

The goal of the Aerodyne DIRTRAN model is two-fold: (1) predict the history of aerosol clouds produced in a battlefield environment (specifically for this report, we discuss dust clouds produced by explosions in soil in different geographic scenarios); (2) predict the time-dependent obscuration at several wavelengths, from the visible to the near IR to mm wavelengths. In the following three sections, we discuss three major elements of the DIRTRAN model, as schematically shown in Figure 2. There is, first, the aerosol source term. In the case of artillery explosions, there are bomb crater dynamics and soil characteristics which must be taken into account in order to have an understanding of the particle ejecta. Next, to adequately account for atmospheric diffusion, the effects of wind, turbulence, and gravity must be included. Finally, the obscuration clutter produced in an EO detection system will be the result of variable extinction, scattering, absorption, and thermal emission from the time-dependent aerosol clouds.

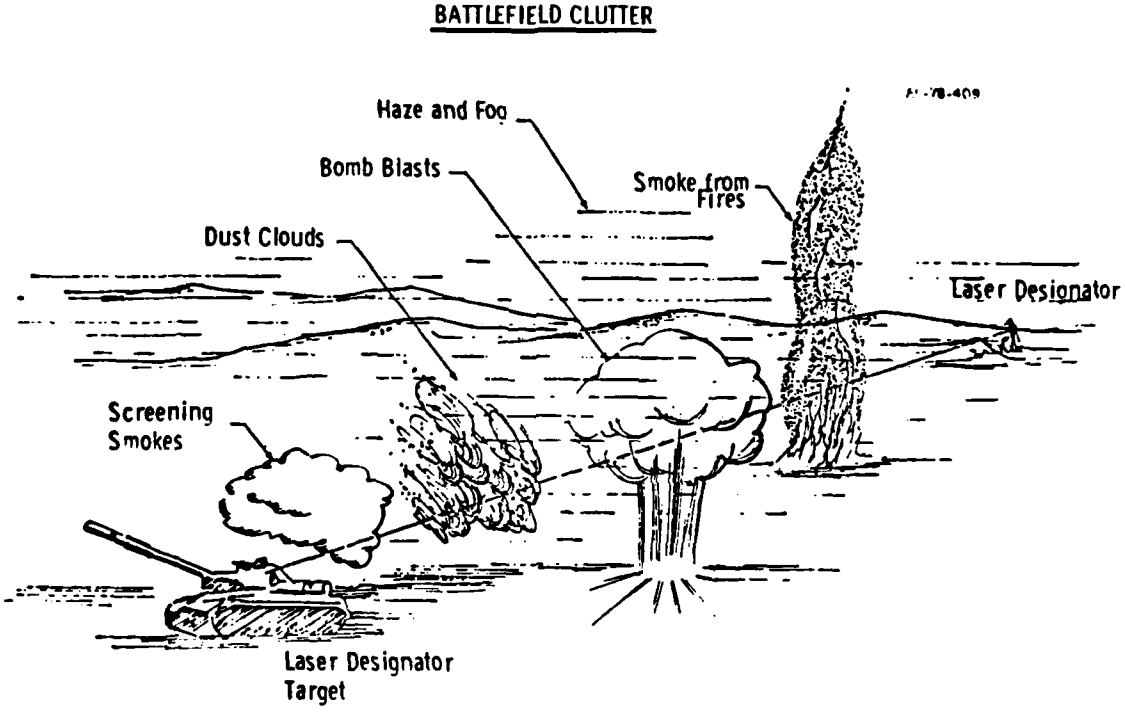

Figure 1. Example of a Clutter in a Battlefield Scenario. This results from the presence of aerosols and turbulence from a variety of sources: dust from explosions, vehicles, and dust storms; screening smokes; fire smoke; fog and haze.

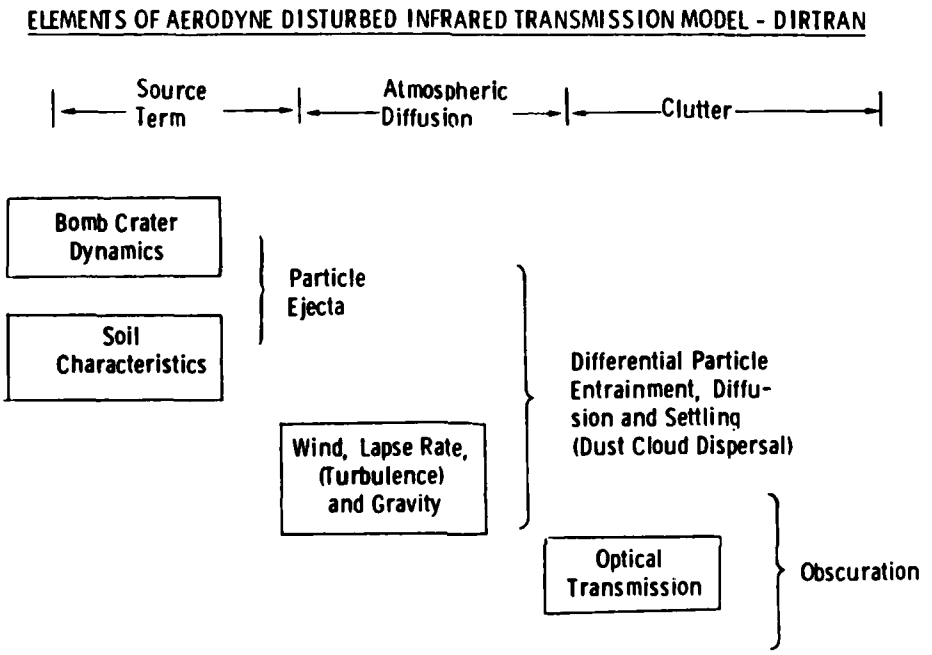

Figure 2. Elements of the Aerodyne DIRTRAN (Disturbed Infrared Transmission) Model. The aerosol source term (e.g., dust resulting from an explosion in soil) is first described. The aerosols are then subjected to atmospheric diffusion resulting from wind, turbulence, and gravitational settling. Finally, the clutter (obscuration and scintillation) of optical radiation is computed.

2. AEROSOL SOURCE TERM: EXPLOSION-PRODUCED DUST

2A. Crater Ejecta

The amount of dust generated by an explosion in soil is obtained from the size of the crater predicted in accord with Ref. (7) as shown in Figures 3 and 4. The particle size distribution function in the ejecta for the smaller radii (<100 μm) is assumed to be log-normal with a mean radius, standard deviation, and mass loading which will be determined from a systematic analysis of data. It is noted that "the process of comminution of the crater material has not been described either theoretically or experimentally" (Ref. (8)). A comparison of soil analysis and dust cloud particulate data will provide insights into this problem. Comparable uncertainty also exists with regard to the initial velocities of the ejecta (Refs. (8) and (9)). Aerodynamic deceleration causes the ejecta to come to rest relative to the air and thus determines the initial conditions for atmospheric diffusion of the dust. This aspect of the problem is important in determining the partitioning of soil ejecta inside and outside the hot gases as discussed below in Section 2C. These will be treated parametrically and compared with data.

2B. Effect of Vegetative Cover on Production of Dust Clouds

Figure 5 shows the results of transmission tests in the 8 - 12 μm band performed by the Army Night Vision & Electro-Optics Laboratory (NV&EOL), Ft. Belvoir, Va. This test -- known as TAPATS (Threat Artillery Preparation Against Tank Sights) was conducted in July 1978 at Ft. Knox, Ky. The transmission data shown are the results of a tank night sight viewing through a 155 mm HE barrage of intensity 0.8 rounds/sec/km. Notable in the figure is the fact that from the first-round impact to several tens of seconds after the barrage ended, the transmission was essentially zero. That is, there were no visibility holes evident for the entire length of the barrage. In Figure 6 is plotted the transmission during a barrage conducted at Grafenwohr, Germany in November 1978 by NV&EOL. In this case, the barrage had an intensity of 1.5 rounds/sec/km. Here, attenuation due to background fog and natural aerosols

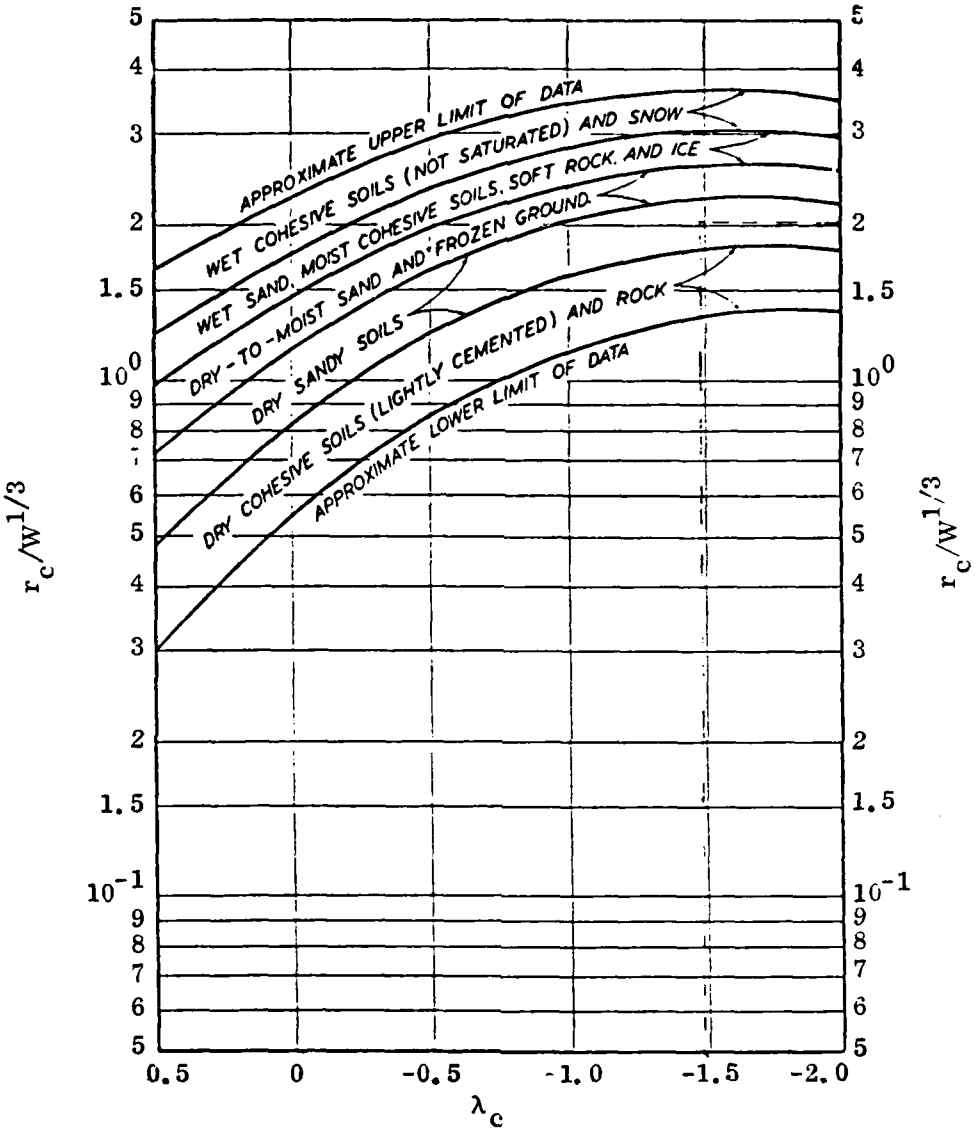

Figure 3. Nomograph for Determining the Apparent Crater Radius R in Various Media (Ref. 7). Here, $\lambda_c = DW^{-1/3}$, where D is explosion depth in feet, and W is the charge weight in pounds of TNT.

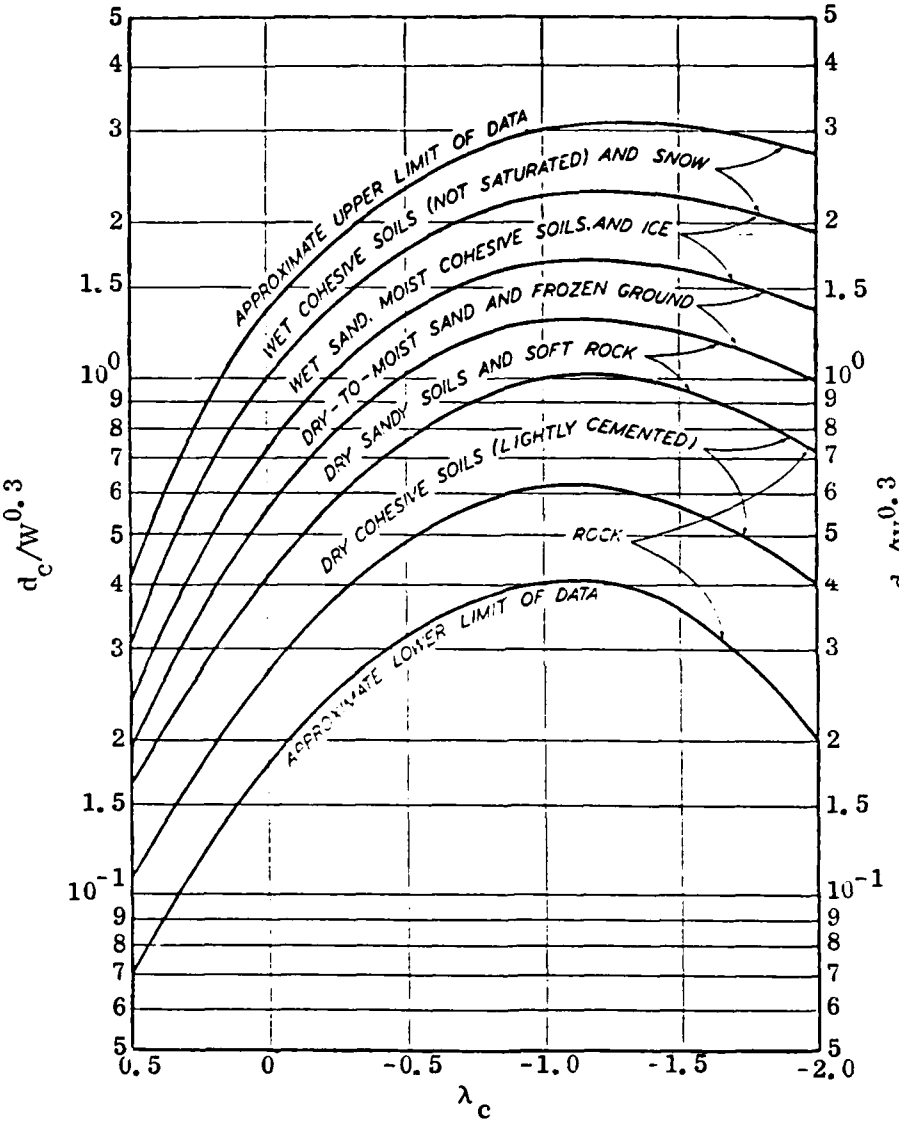

Figure 4. Nomograph Similar to Figure 3 But Used for Determining the Apparent Crater Depth d in Various Media (Ref. 7).

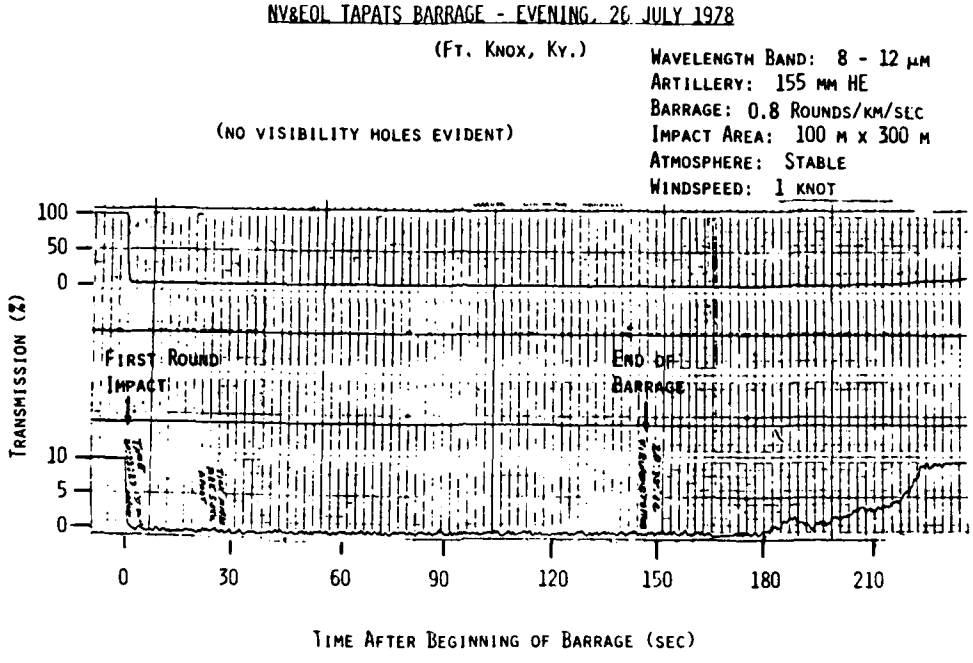

Figure 5. Transmission in the 8 - 12 μm Band During a 155 mm HE Barrage at Ft. Knox, Ky. For this barrage intensity and atmospheric condition, essentially zero transmission was observed for the duration of the barrage and several tens of seconds after it. (Data from the TAPATS test conducted by the Night Vision & Electro-Optics Laboratory, Ft. Belvoir, Va.)

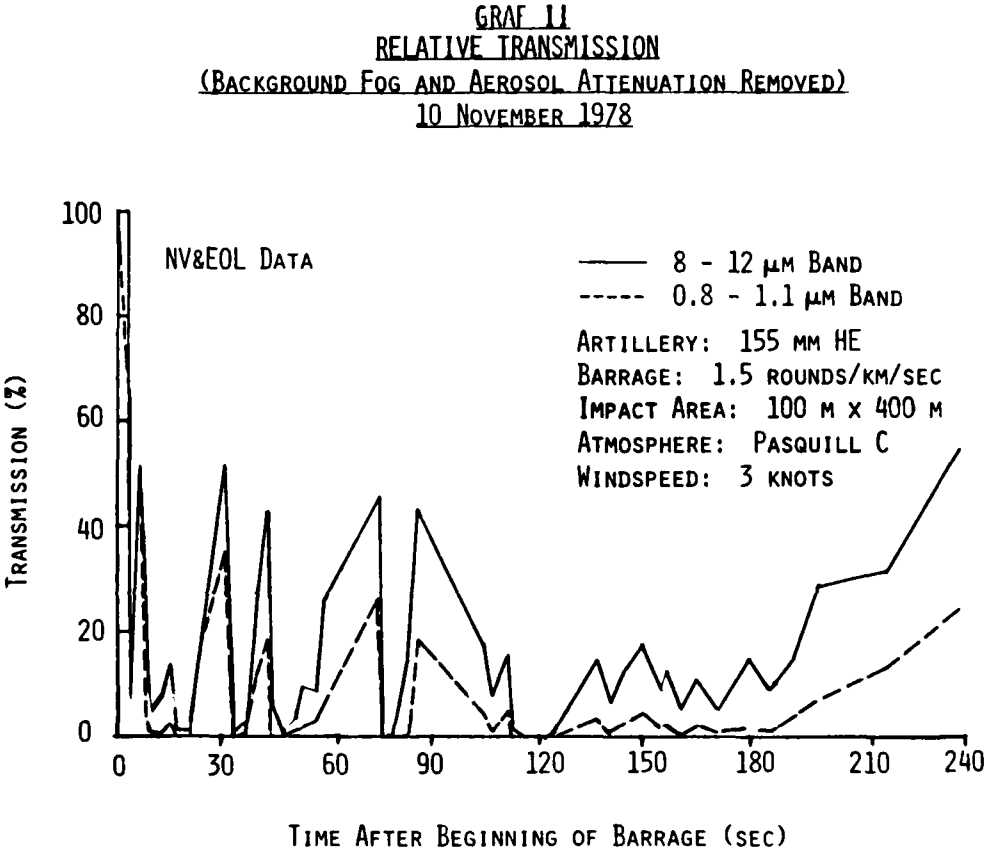

Figure 6. Transmission in the 8 - 12 μm and 0.8 - 1.1 μm Band During a 155 mm HE Barrage at Grafenwohr, Germany. In this situation, visibility holes in excess of 20 - 40% transmission occurred at numerous times during the barrage. (Data from the Graf II test conducted by the Night Vision & Electro-Optics Laboratory, Ft. Belvoir, Va.)

(as determined prior to the barrage) have been removed from the transmission data, so that what is shown in the figure is strictly the changes in transmission due to the barrage. It is evident from the figure that the transmission was considerably in excess of 20 to 40% for several tens of seconds at several different times during the barrage. That is, even with a barrage intensity nearly twice as much as the TAPATS test, the Graf II test transmission was considerably better.

In order to ascertain the reasons for the differences in transmission between the Graf II and TAPATS tests, we looked at a variety of possible circumstances. One of the first things examined was the effect of soil moisture. Table I is a summary of the moisture content of the soil for the TAPATS and Graf II tests. It may be noted that the average moisture content for Zone 4, Grafenwohr (corresponding to Figure 6) was approximately 20%; the moisture content for the TAPATS test was on the order of 16%. That is, the moisture content for both tests were comparable. We were thus led to conclude that soil moisture content was not the primary mechanism for describing the difference in transmission between the TAPATS and Graf II tests.

TABLE I
SOIL MOISTURE CONTENT

Test	Location	Date	Moisture Content
TAPATS	Ft. Knox, Ky.	July 1978	16%
Graf II	Grafenwohr, Germ	Nov. 1978	13 - 27% (Zone 4)
			6.5 - 15% (Zone 1)

We next looked at photographs showing the size of the craters produced in the Graf II tests. Immediately evident is the fact that the depth of the grassy sod is on the order of 25 cm, as shown in Figure 7. Also evident in the figure is the existence of large clumps of sod which have been simply rolled over due to the explosion of the 155 mm high explosive round. Figure 8 is a diagram showing the effect of sod on crater volume. It is drawn approximately according to scale for the crater depth produced by a 155 mm HE round. It may be seen that the sod takes up the upper

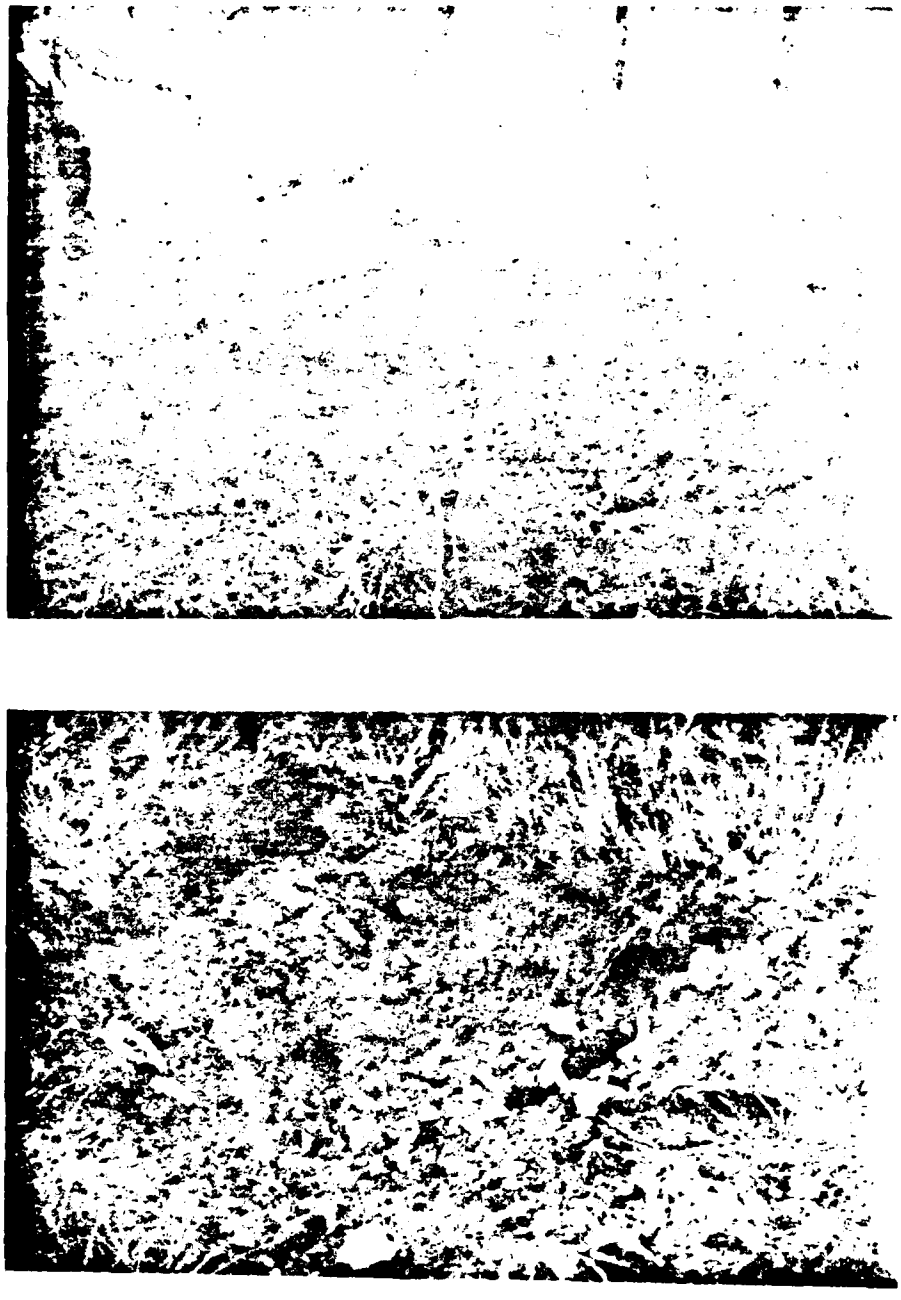

Figure 7. Graf II Test 155 mm HE Round Craters. Depth of vegetative sod cover is approximately 25 cm, comprising a large portion of the crater volume.

EFFECT OF SOD (VEGETATIVE COVER) ON CRATER VOLUME

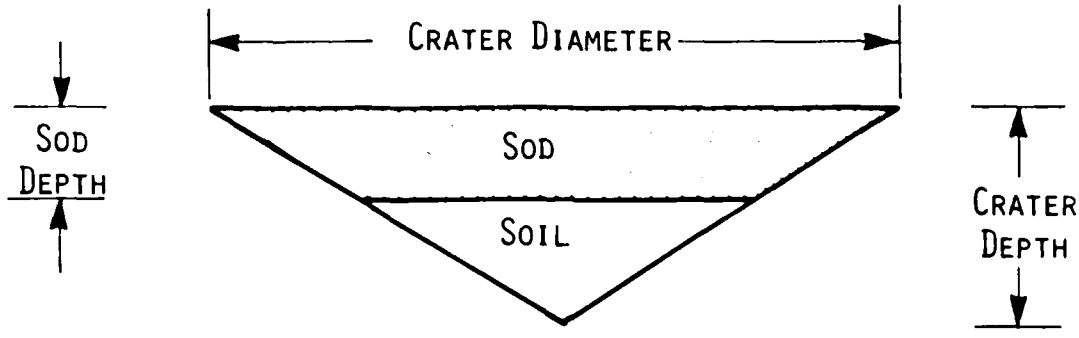

Figure 8. Effect of Sod (Vegetative Cover) on Crater Volume. The sod depth is drawn here roughly to scale for the Graf II test for the 155 mm HE round craters. The volume of soil (which is available for production of entrained dust) is seen to be only a small fraction of the total crater volume.

portion of the crater (where the greatest crater volume occurs). Only a relatively small portion of the total crater volume contains soil particles which might be entrained in the atmosphere. To see this effect mathematically, if we assume the crater volume is conical in shape, then that part of the crater volume V_c which contains only soil (i. e., no sod) is given by the following equation:

$$V_c = \frac{\pi}{3}\left(\frac{r_c}{d_c}\right)^2 (d_c - d_s)^3$$

where r_c and d_c are the crater radius and diameter respectively (as determined in accord with Ref. (7)) and where d_s is the sod depth. It may be noted here that the effect of sod depth comes in as the cube of the difference between the crater depth and the sod depth, i. e., the soil-only crater volume is a very sensitive function of sod depth.

The impact zone for the Ft. Knox TAPATS test is being continually churned up by test barrages. That is, there is no substantial vegetative or sod cover because it is continually being depleted by the explosion of HE rounds. Thus, we are led to the conclusion that the differences in the obscuration between the TAPATS and Graf II data may be attributed to the presence of vegetative soil cover (sod) in the Germany test site, a sod thickness sufficient to prevent much dust entrainment, allowing a considerable number of visibility holes to occur in the transmission data.

2C. Partitioning of Particles Inside and Outside of the Explosion Fireball

Figure 9 is a photograph which was taken during the Dusty Infrared Test I (DIRT I) performed by the Atmospheric Sciences Laboratory, White Sands Missile Range in October 1978. Evident in the photograph is the buoyantly rising cone-shaped or v-shaped hot ball of gases and dust produced by the explosion, i. e., the hot gases and dust first rise into the atmosphere before being dominated by wind diffusion. Surrounding this hot gas at the base is a skirt of dust that is not buoyantly rising and which is immediately subjected to wind diffusion. Thus, both aspects of this aerosol source term must be taken into account with regard to atmospheric diffusion. Figure 10 is also taken from the DIRT I test series. In this case, the explosion has occurred several seconds prior to the taking of the photograph. It may be noted that the hot fireball gases and dust have risen to a higher altitude and that there is a puff at the top of the cloud. Noteworthy also is the fact that the skirt of dust at the base of the cloud is still present. This will have a significant effect on ground-based EO systems.

2D. Initial Hot Gas Cloud

The formation and dispersion of dust clouds produced by artillery explosions involve two distinct sequential phases characterized by two drastically different time scales. In the first phase, formation of the crater and the pressure/velocity equilibration of the detonation products as well as the ejecta occur within times on the order of 10^{-3} to 10^{-2} sec. The DIRTRAN model relies on existing methodology for the state and size of the cloud at the end of this phase. Specifically, the size and temperature of the pressure-equilibrated hot gases are determined from well

established correlations of hydrodynamic blast calculations (Ref. (10)). The second involves subsequent buoyancy and diffusion-controlled dispersion which takes place on time scales on the order of 10^1 to 10^2 sec and is described in Section 3.

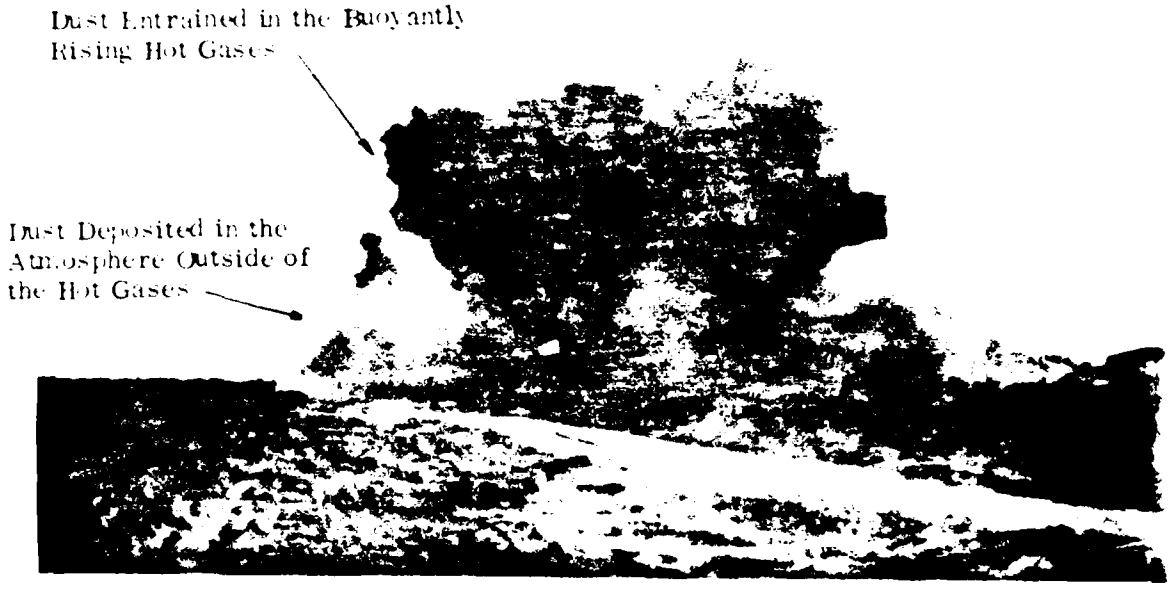

Figure 9. Example of Entrainment Partitioning of Explosion-Produced Soil Ejecta Inside and Outside of Hot Gases From Explosion.

(Data from DIRT I Test series conducted at White Sands Missile Range in October 1978 by the Army Atmospheric Sciences Laboratory.)

Figure 10. Example of Buoyant Rise Effects on the Dispersion of Explosion-Produced Dust Clouds

Also evident is the effect of a mild wind which causes the rising cloud to follow a slanted path. In addition, dust which was not entrained in the hot gases is still present near the explosion point. (Data from the DIRT I Test series.)

3. ATMOSPHERIC DIFFUSION

3A. Buoyant Cloud Rise and Diffusion

The model presented in Ref. (11) for instantaneous point releases are used. Modifications are introduced to accommodate the finite initial cloud size and arbitrary vertical temperature profile of the atmosphere, including the possible existence of an inversion layer. Another modification takes into account the entrainment of dust particles and their setting at their size-dependent terminal velocity relative to the gas cloud.

3B. Wind-Controlled Diffusion

In Figure 11 we show a picture taken at Ft. Sill, Ok. during the Dust/Debris Tests conducted in May 1978 by Dugway Proving Ground at the request of the Project Manager Smoke/Obscurant Office, Aberdeen Proving Ground, MD. Evident in the photograph are three explosions separated in time, each of which shows a strong wind-shear effect, i. e., dust near the ground is not subjected to as much wind advection as dust higher in altitude. This is due to the fact that the wind has an increasing velocity with altitude. Also evident in this picture at the leading edge of the dust clouds is a puff at the top. This may be associated with dust that was entrained in the initial buoyantly rising hot-gas fireball.

It is assumed that the process of wind-controlled diffusion is controlled by the differential equation of diffusion, the action of turbulence being represented on a long-time average basis by the gradient transfer relation. The diffusivities in the three coordinate directions are prescribed consistent with the stability characteristics of the atmospheric boundary layer (Ref. 12). Aerosols are subjected to gravitational settling (at their size-dependent terminal velocity) in addition to diffusion.

The initial cloud is divided into horizontal slices of circular cross section. Since the equations are linear in the particle concentration, the solutions for each slice will be superimposed to produce the final solution. The diffusion of the gas and

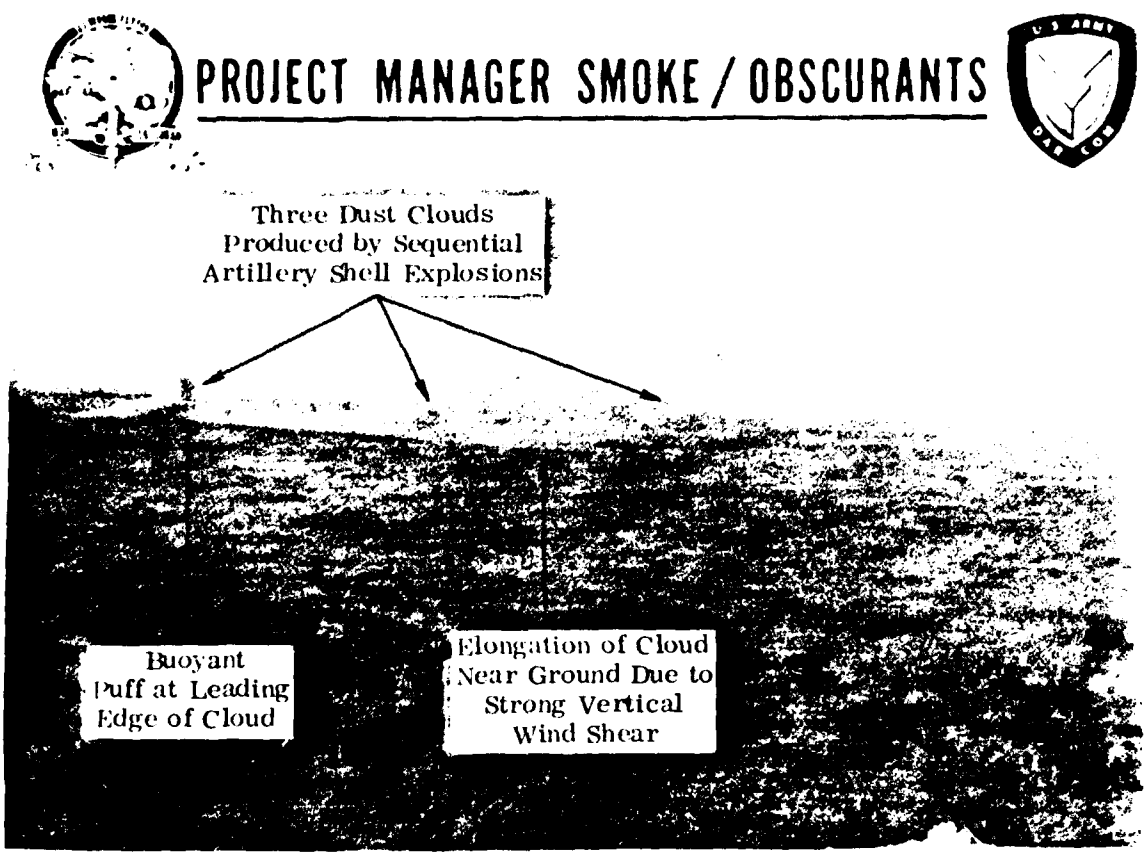

Figure 11. Example of wind-controlled diffusion of dust clouds produced by artillery explosions occurring in the Dust/Debris Test conducted by Dugway Proving Ground at Ft. Sill, Ok, May 1978. The elongation of the cloud along the ground is due to the effect of strong vertical wind shear.

(Photograph courtesy of Col. Henry R. Shelton, Mr. Anthony Van de Wal, and Mr. Eugene Bowman, PM Smoke/Obscurants Office, Aberdeen Proving Ground, Md.)

aerosols contained in each slice is then described by solutions of the diffusion equation obtained by transform methods. Specifically, we consider moments of the particle concentration function $C(x, y, z, t)$, viz.,

$$T_{pq} \equiv \iint_{-\infty}^{\infty} x^p y^q \, C \, dxdy \tag{1}$$

where x is the coordinate in the windward direction. The diffusion equation may be written as

$$\frac{\partial C}{\partial t} + \nabla \cdot \vec{\Gamma} = 0 \tag{2}$$

Here $\vec{\Gamma}$ denotes the particle flux vector with components

$$\Gamma_x = uC - D_x \frac{\partial C}{\partial x} \tag{3a}$$

$$\Gamma_y = - D_y \frac{\partial C}{\partial y} \tag{3b}$$

$$\Gamma_z = - v_g C - D_z \frac{\partial C}{\partial z} \tag{3c}$$

Here u is the wind velocity; D_x, D_y, and D_z are the diffusivities along the x, y, and z directions; v_g is the particle terminal settling velocity. It is important to note that the quantities u, D_x, D_y, and D_z are all allowed to vary with z.

Multiplying Eq. (2) by appropriate powers of x and y and then integrating over all x and y yields the moment equation

$$\left(\frac{\partial}{\partial t} - \frac{\partial}{\partial z} D_z \frac{\partial}{\partial z} - v_g \frac{\partial}{\partial z}\right) T_{pq} = pu \, T_{p-1,q} + p(p-1) D_x T_{p-2,q} + q(q-1) D_y T_{p,q-2} \equiv R_{pq} \tag{4}$$

Solutions for the first several moments, respectively, describe: the mass distribution of dust in the cloud as a function of height Z and time t ($p = q = 0$); its mean along-wind (x) position ($p = 1,\ q = 0$); its mean cross-wind (y) position ($p = 0,\ q = 1$); its along-wind spread ($p = 2,\ q = 0$); and its cross-wind spread ($p = 0,\ q = 2$).

With variables made dimensionless with respect to a length h equal to the height of release, a velocity $\left[D_Z(h)/h\right]$, and a time $\left[h^2/D_Z(h)\right]$; then, the equation for the zeroth moment T_{00}, subject to a diffusivity $D_Z = D_Z(h)Z^n$, initial conditions

$$t = 0\ ,\quad T_{00} = \frac{Q}{h^3}\,\delta(Z-1) \tag{5-a}$$

and boundary conditions

$$Z = 0\ ,\quad Z^n(\partial T_{00}/\partial Z) = 0 \tag{5-b}$$

$$Z \to \infty\ ,\quad T_{00} \to 0\ , \tag{5-c}$$

can be solved in closed form if $v_g = 0$ to obtain

$$T_{00}(Z,t) = \frac{Q}{h^{3(2-n)}}\,\frac{Z^{(1-n)/2}}{t}\,\exp\left[-\frac{Z^{2-n}+1}{(2-n)^2 t}\right] I_{(n-1)/(2-n)}\left[\frac{2Z^{1-n/2}}{(2n)^2 t}\right] \tag{6}$$

where $I_{(n-1)/(2-n)}$ denotes the modified Bessel function of the first kind of order $\left[(n-1)/(2-n)\right]$.

If $v_g \neq 0$, a closed form expression for the zeroth moment is obtained by heuristic matching of two asymptotic solutions obtained by the following process. The equation

$$\frac{\partial T_{00}}{\partial t} - \frac{\partial}{\partial Z}\left[Z^n\,\frac{\partial T_{00}}{\partial Z} + \alpha\, T_{00}\right] = 0\ , \tag{7}$$

where $\alpha \equiv v_g h/D_Z(h)$, is recast in terms of the independent variables,

$$\xi \equiv Z + \alpha t - 1\ ,\qquad \tau \equiv t$$

to obtain

$$\frac{\partial T_{00}}{\partial \tau} - \frac{\partial}{\partial \xi}\left[(\xi - \alpha\tau + 1)^n \frac{\partial T_{00}}{\partial \xi}\right] = 0 \qquad (8)$$

In turn, Eq. (8) is approximated by

$$\frac{\partial T_{00}}{\partial \tau} - \frac{\partial}{\partial \xi}\left[(1 + \xi)^n \frac{\partial T_{00}}{\partial \xi}\right] = 0 \qquad (9\text{-a})$$

in $\xi >> \alpha\tau$, and by

$$\frac{\partial T_{00}}{\partial \tau} - (1 - \alpha)^n \frac{\partial^2 T_{00}}{\partial \xi^2} = 0 \qquad (9\text{-b})$$

in $\xi >> \alpha\tau$. The solution to Eq. (9-a), subject to the initial and boundary conditions (Eqs. (5-a, b, c)), is readily transposed from Eq. (6), viz.,

$$T_{00}^{(0)}(\xi, \tau) = \frac{Q}{h^{3(2-n)}} \frac{(\xi+1)^{(1-n)/2}}{\tau} \exp\left[-\frac{(\xi+1)^{2-n}+1}{(2-n)^2 \tau}\right] \times I_{(n-1)/(2-n)}\left[\frac{2(\xi+1)^{1-n/2}}{(2-n)^2 \tau}\right] \qquad (10\text{-a})$$

The solution to Eq. (9-b), subject to the initial condition Eq. (5-a), the requirement of boundedness as $\xi \to \pm \infty$, and the restriction $(1 - \alpha\tau) \geq 0$, takes the classical Laplace form

$$T_{00}^{(i)}(\xi, \tau) = \frac{Q}{h^3} \tilde{\tau}^{-1/2} \exp\left[-\frac{\xi^2}{4\tilde{\tau}}\right] \qquad (10\text{-b})$$

where $\tilde{\tau} \equiv \int_0^\tau (1 - \alpha\tau)^n \, d\tau$. A heuristic composite solution to Eq. (8), valid in $Z \geq 0$ and $\tau \leq \alpha^{-1}$, may then be written as

$$T_{00}(\xi, \tau, \alpha) = f(\xi, \alpha\tau)\, T_{00}^{(i)}(\xi, \tau) + \left[1 - f(\xi, \alpha\tau)\right] T_{00}^{(0)}(\xi, \tau) \quad . \qquad (11)$$

Here, $f(\xi, \alpha\tau)$ denotes a suitably selected weight function (see below) satisfying the requirements $f \longrightarrow 0$ in $\xi \gg \alpha\tau$, $f \longrightarrow 1$ in $\xi \ll \alpha\tau$.

A judicious choice of the function $f(\xi, \alpha\tau)$ is obtained upon a study of the exact solution of Eq. (7) for the special case $n = 1$, i.e., the case of neutral stratification, where the diffusivity varies linearly with the height Z. In that case, the change of dependent variable

$$\widetilde{T}_{00}(Z, t) \equiv Z^{\alpha}\, T_{00}(Z, t)$$

leads to the equation

$$Z^{-\alpha} \frac{\partial \widetilde{T}_{00}}{\partial t} - \frac{\partial}{\partial Z}\left[Z^{1-\alpha} \frac{\partial \widetilde{T}_{00}}{\partial Z}\right] = 0 \qquad (12)$$

with solution, subject to the initial and boundary conditions (Eqs. (5-a, b, c)),

$$\widetilde{T}_{00}(Z,t) = Z^{\alpha} T_{00}(Z,t) = \frac{Q}{h^3} \frac{Z^{\alpha/2}}{t} \exp\left[-\frac{Z+1}{t}\right] I_{\alpha}\left[\frac{2Z^{1/2}}{t}\right] \quad . \qquad (13)$$

Whereas the solutions given by Eqs. (10-a, b) are also known, the weight function $f(\xi, \alpha\tau)$ is readily determined upon comparison of Eqs. (11) and (13). If this result, strictly obtained for $n = 1$, is adopted throughout the practical range of values $0 < n \lesssim 4/3$ associated with stable to unstable stratifications, the closed form solution Eq. (11) for the zeroth moment becomes completely defined. The availability of this solution substantively simplifies the determination of the higher moments along the lines presented below.

Returning to Eq. (4), we note that the same differential operator appears in the equations for all the moments. However, while the equation for T_{00} is homogeneous, those for the higher moments include known forcing functions R_{pq}. Whereas the initial conditions are: $t = 0$, $T_{00} \propto \delta(Z - 1)$, and $T_{pq} = 0$; the solution Eq. (11) for

T_{00} provides the Green's function required to construct solutions for the higher moments by superposition. Specifically, if we let

$$G(\xi, \xi', \tau, \tau', \alpha) \equiv$$

$$f\left[\xi - \xi', \alpha(\tau - \tau')\right] \left[\tilde{\tau} - \tilde{\tau}'\right]^{-1/2} \exp\left[-\frac{(\xi - \xi')^2}{4(\tilde{\tau} - \tilde{\tau}')}\right]$$

$$+ \left\{1 - f\left[\xi - \xi', \alpha(\tau - \tau')\right]\right\} \frac{\left[(\xi+1)(\xi'+1)\right]^{(1-n)/2}}{(2-n)(\tau - \tau')} \exp\left[-\frac{(\xi+1)^{2-n} + (\xi'+1)^{2-n}}{(2-n)^2 (\tau - \tau')}\right]$$

$$\times I_{(n-1)/(2-n)}\left[\frac{2(\xi+1)^{1-n/2}(\xi'+1)^{1-n/2}}{(2-n)^2 (\tau - \tau')}\right] \quad , \tag{14}$$

then, the solution for the general moment becomes

$$T_{p,q}(\xi, \tau) = \int_{\alpha\tau - 1}^{\infty} d\xi' \int_0^{\tau} R_{p,q}(\xi', \tau') \, G(\xi, \xi', \tau, \tau', \alpha) \, d\tau' \quad , \tag{15}$$

which can be readily evaluated by numerical integration.

A matrix of solutions given by Eq. (15) covering the ranges of the parameters n and α associated with Pasquill stability categories A through F and dust particle sizes $D \leq 100$ μm have been evaluated. The results in tabular form are included in the DIRTRAN-I code together with interpolation routines which permit determination of the solutions for intermediate values of the parameters. By this process, the calculation of the dust concentration within a given dust size bin at a prescribed space/location and time achieves the same simplicity as the evaluation of a Gaussian.

A typical sequence of particle concentration-length product (relative line-of-sight concentration integrals, i.e., Cf values) contours as computed by the DIRTRAN model is shown in Figure 12 for a sphere of initial radius 5m (corresponding roughly to a 155 mm HE artillery shell explosion) centered at x = 0 and z = 5m. The times plotted

are 5, 10, 30, and 50 sec after detonation in Figure 12 for purely wind-controlled case and in Figure 13 for the initially buoyancy controlled case. In both cases, a wind speed of 3 m/sec (measure at height of 10m above the ground) was used. Figure 12 is the result of calculations for the case of small particles, i.e., no gravitational settling. Figure 13 shows the results for particles of nominal diameter 50 μm and a nominal gravitational settling velocity of 18 cm/sec. Figure 14 shows the superposition of an initially buoyancy-dominated case (which is subsequently wind controlled) with the immediately wind dominated case, both for the situation of small particles. Noteworthy, in Figure 14 is the development of a stretched-out cloud hugging the ground, quite similar to that manifested in the data of Figure 11.

In conclusion, we submit that the DIRTRAN model reproduces the salient features of dust clouds in a battlefield scenario. Detailed validation with data from the DIRT I and Graf II test series is being actively pursued at the present time.

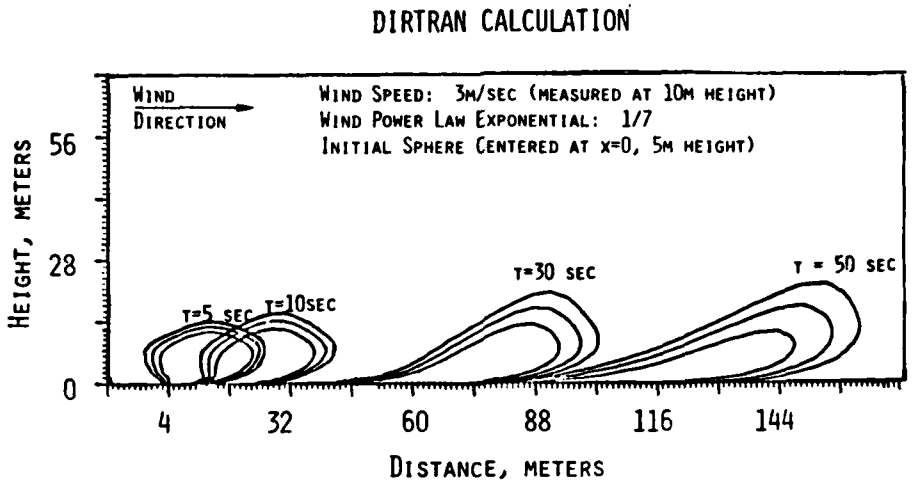

Figure 12. Wind controlled aerosol dispersion. Time sequence of contours of line-of-sight integrals of dust concentration per unit area (i.e., $C\ell$ values) computed by the DIRTRAN model for the case of no initial buoyancy. Note the effect of wind shear. Particles are assumed small (i.e., negligible gravitational settling). The three concentric contours represent respectively, 0.1, 0.05, and 0.025 fractions of the initial average line-of-sight integral of particle concentration.

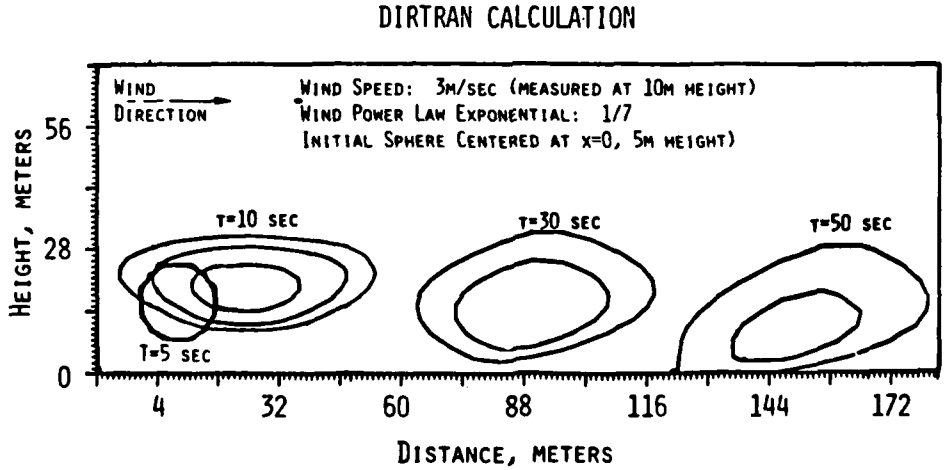

Figure 13. Buoyancy diffusion of aerosols with wind and gravitational settling (50 μm diameter particles). Note that for $t \geq 30$ sec, the dust cloud has sufficiently diffused that the 0.1 fraction contour no longer exists.

DIRTRAN CALCULATION

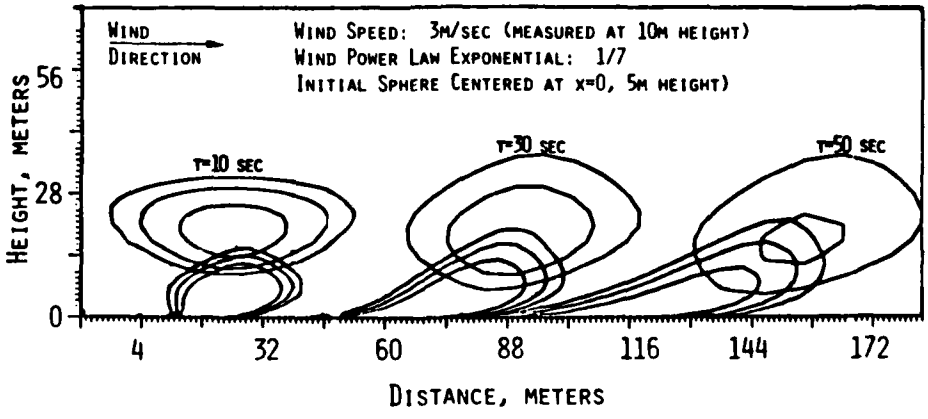

Figure 14. Superposition of wind and buoyancy controlled diffusion of small particles. Note the strong wind shear effect with altitude, an important phenomenon for near-ground line-of-sight obscuration effects.

4. IR CLUTTER

In addition to total obscuration of a target of interest by battlefield-induced contaminants, there is the serious problem of battlefield clutter produced by these particulates as well as associated turbulence. In this situation, there may be so much spatial and temporal variation in a detector field of view due to $C\ell$ (aerosol concentration-length product) or thermal changes that a target may not be readily discernible. This can happen even though the target may not be completely obscured. This clutter can result in visibility holes at infrared wavelengths and scintillation at mm wavelengths. This was especially evident in the Graf II tests with tank night sights operating in the 8 - 12 μm region. At mm wavelengths, results from the DIRT I tests [13] showed that scintillation could be a factor of three greater than the average attenuation. These marginal seeing conditions pose serious threats to electro-optical systems, and an understanding of the reasons for and the probability of their occurrence is essential if one is to ascertain system effectiveness. We suggest here that the existence of battlefield clutter may be attributed to the interplay of barrage intensity (be it high explosive or smoke rounds) and large atmospheric eddies of characteristic period and size.

Inspection of available transmissometer data forcibly exhibits the existence of distinct transmission windows (visibility holes) in battlefield-induced obscurants under marginal seeing conditions. The visibility holes under these barrage conditions can be explained by the presence of large atmospheric turbulent eddies. In the temporal domain, these transmission events have typical individual durations on the order of ten seconds and repetition rates on the order of one minute. In the spatial domain, the characteristic wavelength is of the order of 150m between events, and the scale of each event is on the order of 30m. The data in Figure 15 show the visibility holes observed during the Ft. Knox TAPATS test conducted by NV&EOL in July 1978. The optical transmission level between these holes is relatively monotone in time; the ac component of the transmission, however, is dominated by large atmospheric eddies which are of well defined scale (size) and frequency and not by a spectrum of random

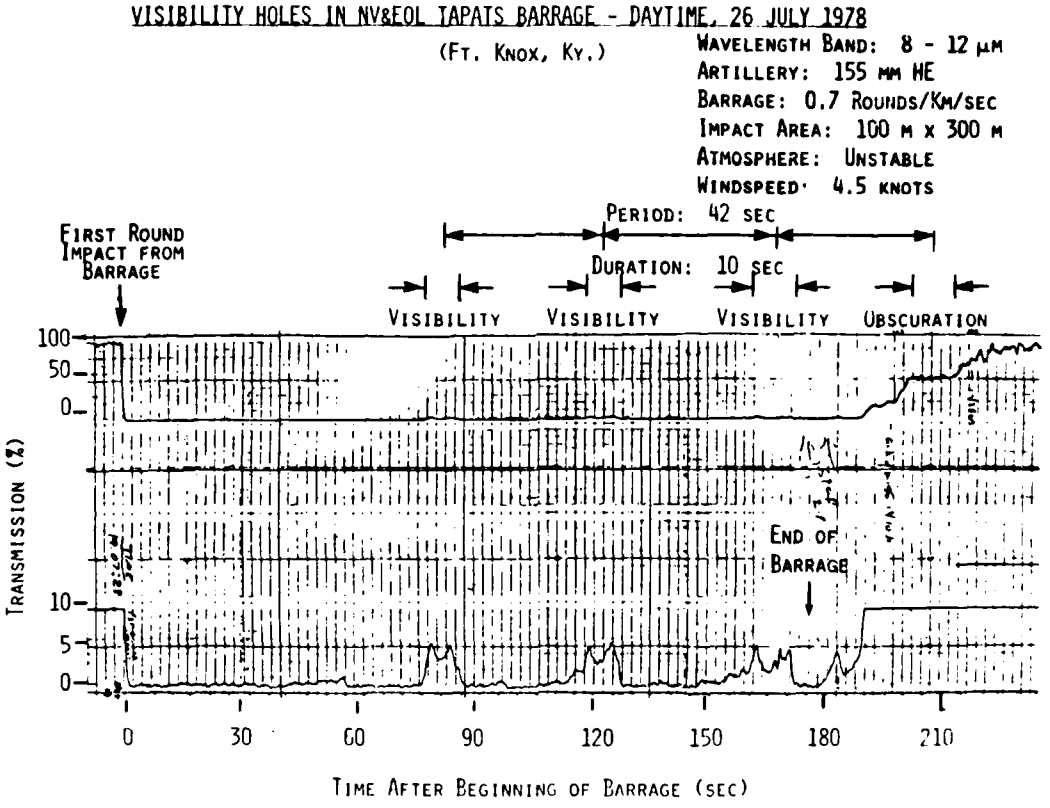

Figure 15. Effect of large-eddy turbulence on visibility holes. Periodicity of 42 sec and duration of 10 sec per event is evident. This cannot be explained by the barrage itself which was an average of one round every five seconds in rapid random fire from an artillery battery of six guns. (The probability is negligible that the random rounds would land in the same place with respect to the line of sight at precisely the same interval and duration at three different times during the barrage. In addition, there is another hole (an obscuration hole) occurring after the barrage and which is of the same periodicity and duration as the other three holes.)

(turbulent) scales and frequencies. A deterministic model descriptive of the nature, scale, and frequency of these dominant eddies is required to predict the occurrence of the windows and, therefore, the nature of clutter to be encountered in a battlefield under the conditions of marginal viewing.

The influence of large eddies on specific measurements of obscuration is also clearly manifested in other currently available data. The data in Figures 16 to 19 are from the DIRT I tests. The pictures on the fire smoke obscurant clouds show markedly different cloud patterns with different lengths and frequencies as mentioned above. A comparison of the pictures also suggests that validation of any obscuration model will be prevented by the limited number of data available and the consequent inability to determine the "attendant statistics". We wish to point out that the narrow bandwidth of the large-eddy effects (i. e., the presence of a well defined characteristic frequency for a given meteorological condition) clearly shows two options for model validation: 1) the repetition of the same measurement for a statistically meaningful number of events (> 10 to 100) and subsequent ensemble averaging of the results at fixed meteorological condition and obscurant source; or 2) the analytical prediction of the variance in the observations produced by the large turbulent eddies.

We conclude that an understanding of the interplay between barrage intensity and large atmospheric eddies of characteristic period and size will provide insights to the problem of battlefield clutter, scintillation, and the existence of visibility holes. At present, we are directing efforts toward resolving this problem.

Figure 16. Example of visibility holes produced by the interplay of large-eddy turbulence effects and fire smoke generation on obscuration. (Tests performed during the DIRT I series.)

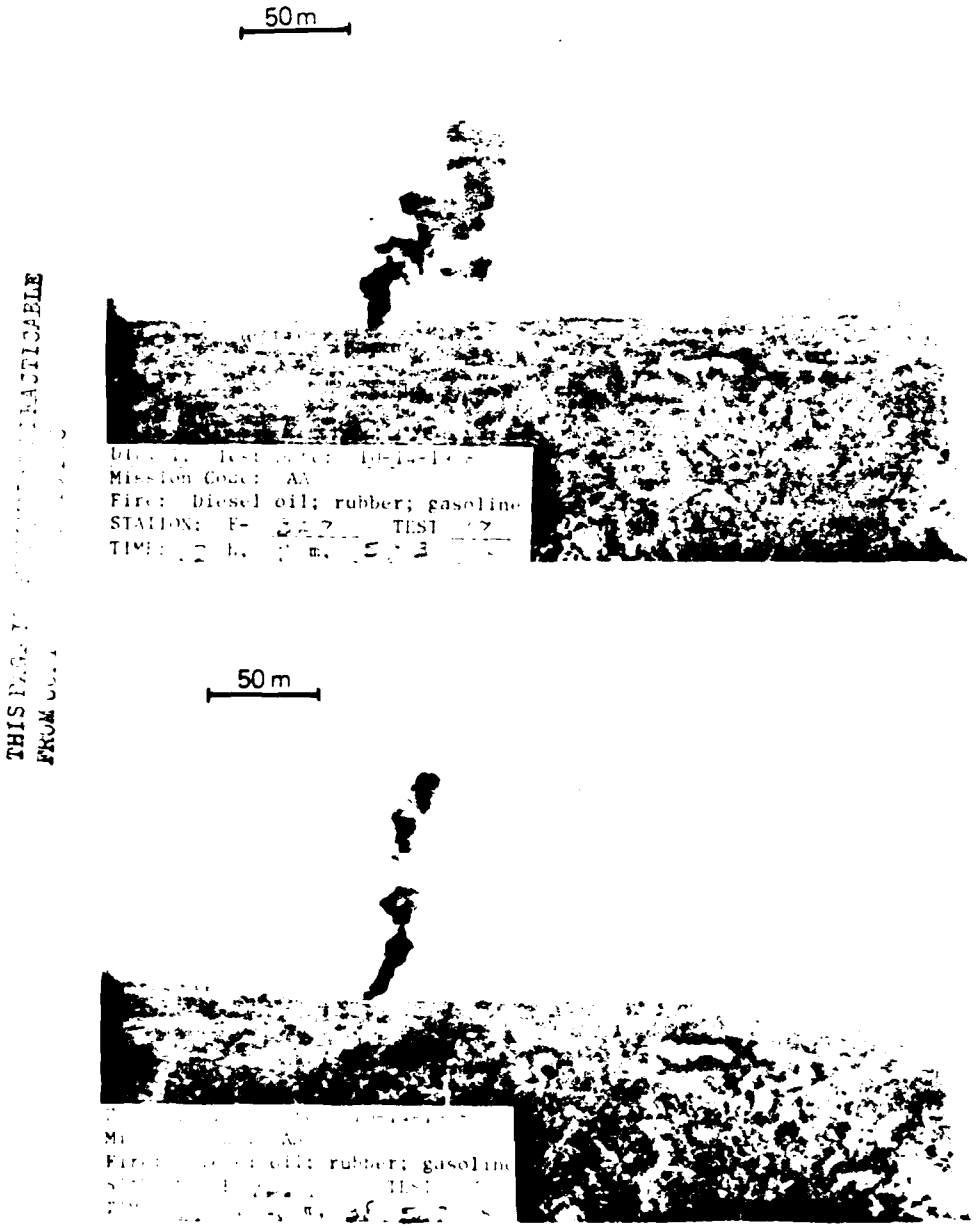

Figure 17. Two pictures of buoyantly rising smoke separated in time by approximately 40 sec. In the lower event, the large-eddy turbulence is sufficient to completely offset (nullify) the rise of the smoke due to buoyancy from the hot gases produced in the fire. In this situation, a visibility hole is created at an altitude of about 70m. (Data from DIRT I.)

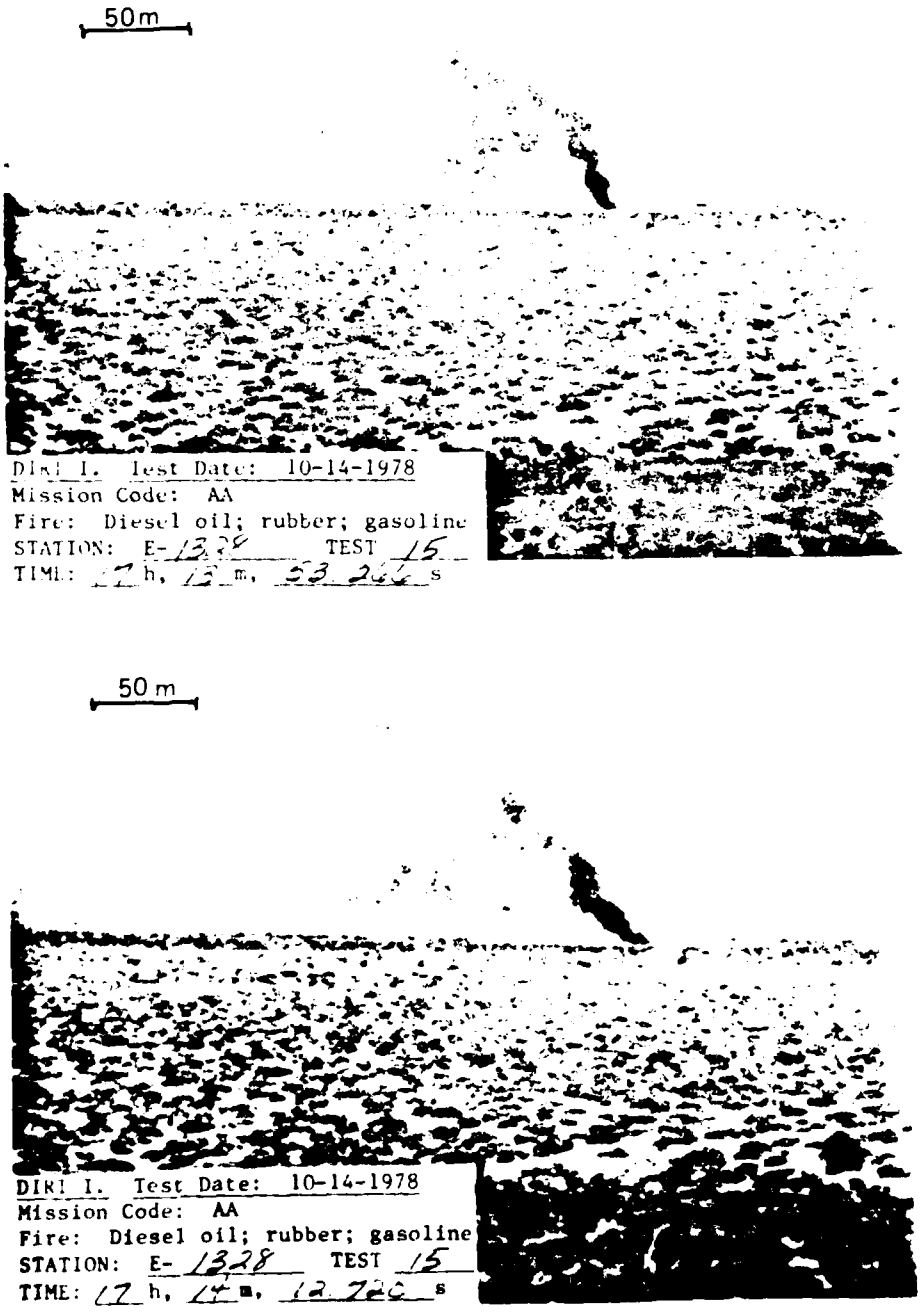

Figure 18. Example of bifurcation of DIRT I fire smoke clouds due to large atmospheric eddies separated in time by approximately 20 sec. A visibility hole between the two plumes at an altitude of 40m is evident. Obscuration effects at ground level are also evident.

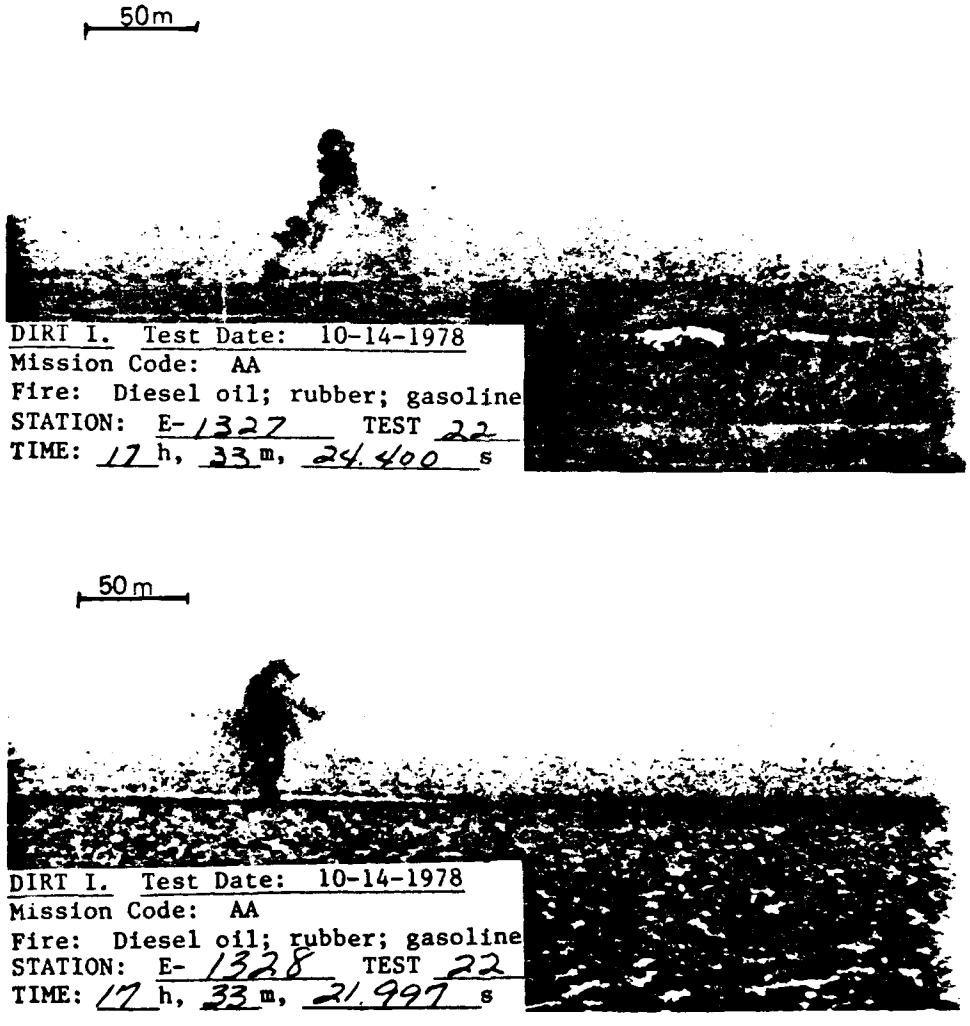

Figure 19. View of approximately the same "wishbone" fire smoke event (temporal separation of less than 2.5 sec) from two different aspects (angular separation of 64.2°). In the upper picture the large-eddy turbulence has more than offset the buoyant rise of the cloud, i.e., the smoke has been forced back to the ground creating visibility blockage along the ground (zero altitude) at a distance of 40m from the fire smoke source. A visibility window is evident 20m laterally from the source near the center of the "wishbone" smoke distribution. In the lower picture, no visibility windows are evident whatsoever due to the different aspect angle. (Data from DIRT I.)

5. SUMMARY AND CONCLUSIONS

For the dust aerosol source term, we conclude that dust particles inside and outside of the explosion-produced fireball have different diffusion mechanisms and obscure in different regions of the atmosphere as evidenced by DIRT I data; they, thus, need to be accounted for separately and then superimposed. We also conclude that the large differences in obscuration between the Ft. Knox TAPATS (Threat Artillery Preparation Against Tank Sights) test and the Grafenwohr Graf II test may be attributed to the existence of thick (≈ 25 cm) vegetative cover (sod) at Grafenwohr, resulting in a smaller amount of entrained soil particles. For the atmospheric diffusion, we discuss provisions in the DIRTRAN model for analytic solutions (which run fast on the computer) to the atmospheric diffusion equations which account for: vertical wind shear (important for near-ground line-of-sight obscuration effects); variable vertical diffusivities with altitude (important for different atmospheric stability categories); and gravitational settling (important for large dust particles). It is observed that these solutions realistically model the time-dependent cloud shape of battlefield aerosols. Finally, we show that the existence of battlefield clutter which occurs in a barrage is the result of the interplay of barrage intensity and large atmospheric eddies of characteristic period and size. This has a strong dependence on stability category, and produces visibility holes at IR wavelengths and scintillation at mm wavelengths.

Acknowledgements

This research has been technically monitored by Dr. Louis Duncan of the Army Atmospheric Sciences Laboratory, White Sands Missile Range, N.M. The effort and conclusions reported here have greatly benefited from continuing technical exchanges with Drs. Louis Duncan and Franklin Niles of ASL, and with Ms. Luanne Obert, Mr. Russell Moulton, and Mr. Thomas Cassidy of the Army Night Vision & Electro-Optics Laboratory, Ft. Belvoir, Va. For this, the authors express their sincere appreciation. The technical discussions with Drs. Morton Camac and Wai Cheng of Aerodyne are also gratefully acknowledged. The authors also acknowledge support of this research through the Scientific Services Program, Battelle Columbus Laboratories, Durham Operations, Durham, N.C., and the Army Research Office, Research Triangle Park, N.C.

References

1. J. F. Ebersole, M. Camac, V. Yousefian, J. Draper, and D. Robertson, "Munitions Signatures: Review and Recommendations (U)," ARI-RN-100, ARI-Doc. No. 77-2670, Report for Defense Advanced Research Projects Agency (DOD), September 1977 (SECRET).

2. J. F. Ebersole, "Use of Aerosol Screens to Obstruct Intelligence Collection (U)," ARI-Doc. No. 79-3278 and 78-2967, Report for Air Force Foreign Technology Division, April 1978 (SECRET).

3. J. F. Ebersole, "DIRT I ASL Battlefield Dust Tests -- Predictions and Recommendations," Final Tech. Rpt.prepared for Army Atmospheric Sciences Laboratory, 27 October 1978.

4. J. F. Ebersole, "Dust Cloud Motion and Obscuration Predictions of Grafenwohr II Realistic Battlefield Sensor Trials," Rpt. prepared for Army Night Vision & Electro-Optics Laboratory, 25 October 1978.

5. J. F. Ebersole, R. Vaglio-Laurin, D. S. Dvore, M. Martinez-Sanchez, W. K. Cheng, and L. D. Duncan, "Preliminary Model Validation Analysis Using Data from the DIRT I and Graf II Battlefield Dust Obscuration Tests (U)," Proc. Symp. Smoke/Obscurants III, April 1979 (CONFIDENTIAL).

6. J. F. Ebersole, R. Vaglio-Laurin, M. Camac, L. P. Obert, and L. D. Duncan, "Analysis of Recent Infrared Obscuration Army Artillery Dust Field Tests (U)," Proc. 27th National Infrared Information Symp., May 1979 (SECRET).

7. "Cratering from High Explosive Charges: Analysis of Crater Data," Tech. Rpt. No. 2-547, Report 2, June 1961, U. S. Army Engineer Waterways Experiment Station, Corps of Engineers, Vicksburg, Miss.

8. W. R. Seebaugh, "A Dynamic Crater Ejecta Model," Impact and Explosion Cratering (Pergamon, New York, 1977), D. J. Roddy, R. D. Pepin, and R. B. Merrill, eds., pp. 1043 - 1056.

9. R. J. Andrews, "Characteristics of Debris from Small-Scale Cratering Experiments," Impact and Explosion Cratering (Pergamon, New York, 1977), D. J. Roddy, R. D. Pepin, and R. B. Merrill, eds., pp. 1089 - 1100.

10. J. Thompson, "S-Shock Code," Report GE75TMP-14, General Electric - TEMPO, March 1975.

11. B. R. Morton, G. Taylor, and J. S. Turner, "Turbulent Gravitational Convection from Maintained and Instantaneous Sources," Proc. Roy. Soc. A, 234, 1-23, 1956.

References (Cont.)

12. F. Pasquill, Atmospheric Diffusion, 2nd ed. (Wiley, New York, 1974).

13. D. Snider, R.W. McMillan, and J.J. Gallagher, "Millimeter Wavelength Transmission Measurements," Measured Effects of Battlefield Dust and Smoke on Visible, Infrared, and Millimeter Wavelength Propagation: A Preliminary Report on Dust Infrared Test - I (DIRT-I), Atmospheric Sciences Laboratory Report ASL-TR-0021, January 1979, compiled by J. Lindberg.

U.S. GOVERNMENT PRINTING OFFICE: 1980 — 677-119/53